

Supplementary Information:

Hot electron and hole dynamics in thiol-capped CdSe quantum dots revealed by 2D electronic spectroscopy

Nils Lenngren,[†] Mohamed A. Abdellah,^{†,‡} Kaibo Zheng,^{†,¶} Mohammed J.
Al-Marri,[¶] Donatas Zigmantas,[†] Karel Žídek,^{†,§} and Tõnu Pullerits^{*,†}

[†]*Department of Chemical Physics, Lund University, PO Box 124, 221 00 Lund, Sweden*

[‡]*Department of Chemistry, Qena Faculty of Science, South Valley University, Qena 83523,
Egypt*

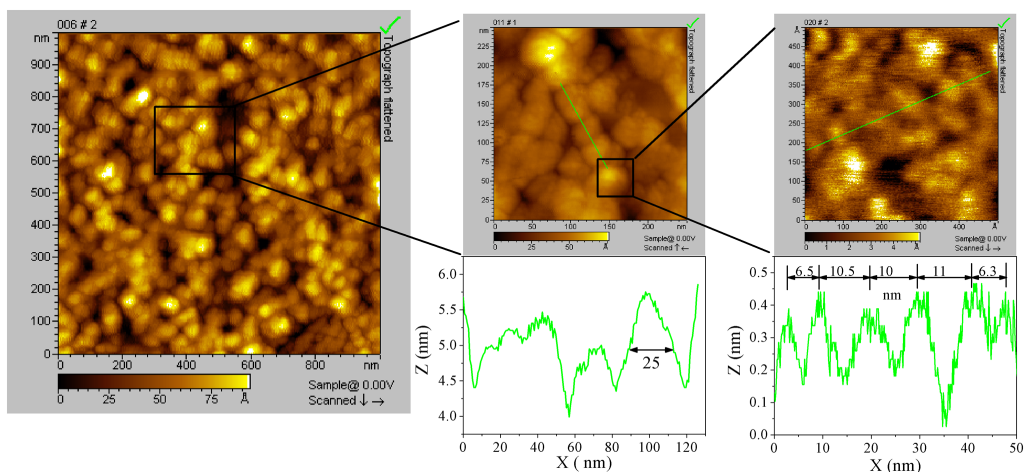
[¶]*Gas Processing Center, College of Engineering, Qatar University, PO Box 2713, Doha,
Qatar*

[§]*Regional Centre for Special Optics and Optoelectronic Systems (TOPTEC), Institute of
Plasma Physics, Academy of Sciences of the Czech Republic, Za Slovankou 1782/3, 182 00
Prague 8, Czech Republic.*

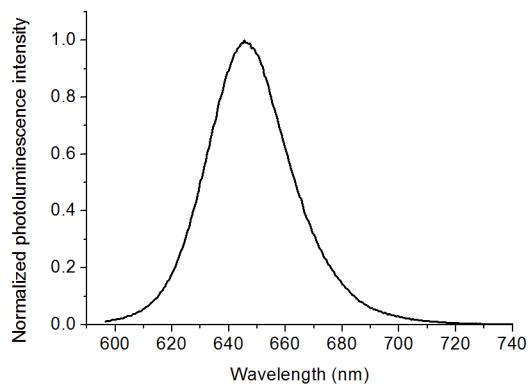
E-mail: tonu.pullerits@chemphys.lu.se

SI-1. Sample characterization

The size of the quantum dots was determined from the position of the first absorption peak by using the equation of Yu et al.¹ It was further confirmed by atomic force microscopy (see SI-Figure 1). The photoluminescence spectrum of the QDs was also measured (see SI-Figure 2). The fluorescence quantum yield of the QDs after ligand exchange was below 10%. The crystal structure of similar QDs prepared by our group has been determined by X-ray diffraction to be zincblende.²



SI-Figure 1: Atomic force microscopy of a mixture of QDs – the ones used in the paper (first absorption peak at 635 nm in room temperature) and smaller QDs (first absorption peak at 493 nm). The large particle across the green line in the right panel is a 635 nm QD.



SI-Figure 2: Photoluminescence spectrum of the QDs used.

SI-2. Average number of excitons per QD ($\langle N \rangle$)

The average number of excitons per QD $\langle N \rangle$ was calculated to ensure that multiple excitons are not formed. The calculation is broadly similar to the description in the supporting information of a previous paper from our group,³ but a misprint there is corrected in the following.

$\langle N \rangle$ is given by multiplying the photon fluence f (in photons per cm^2 per pulse) by the absorption cross section σ (in cm^2):

$$\langle N \rangle = f\sigma \quad (1)$$

The photon fluence is calculated from the energy per pulse (1 nJ), the beam diameter (100 μm), and the central wavelength (600 nm). The absorption cross section is calculated from the extinction coefficient at the first exciton peak ϵ_{1S} (in $\text{M}^{-1} \text{cm}^{-1}$) given by the equations of Yu et al.¹ and rescaled to 600 nm using the absorption spectrum measured at 77 K:

$$\sigma = \frac{A_{600}}{A_{1S}} \frac{\epsilon_{1S} 1000 \text{ cm}^3/\text{L}}{N_A} \ln 10 \quad (2)$$

where A_{600}/A_{1S} is 0.931, ϵ_{1S} is $8.3 \cdot 10^5 \text{ M}^{-1} \text{cm}^{-1}$ from a first exciton peak at 635 nm, and N_A is the Avogadro constant (in mol^{-1}). Putting this together yielded $\langle N \rangle = 0.12$.

SI-3. The 2D experiment

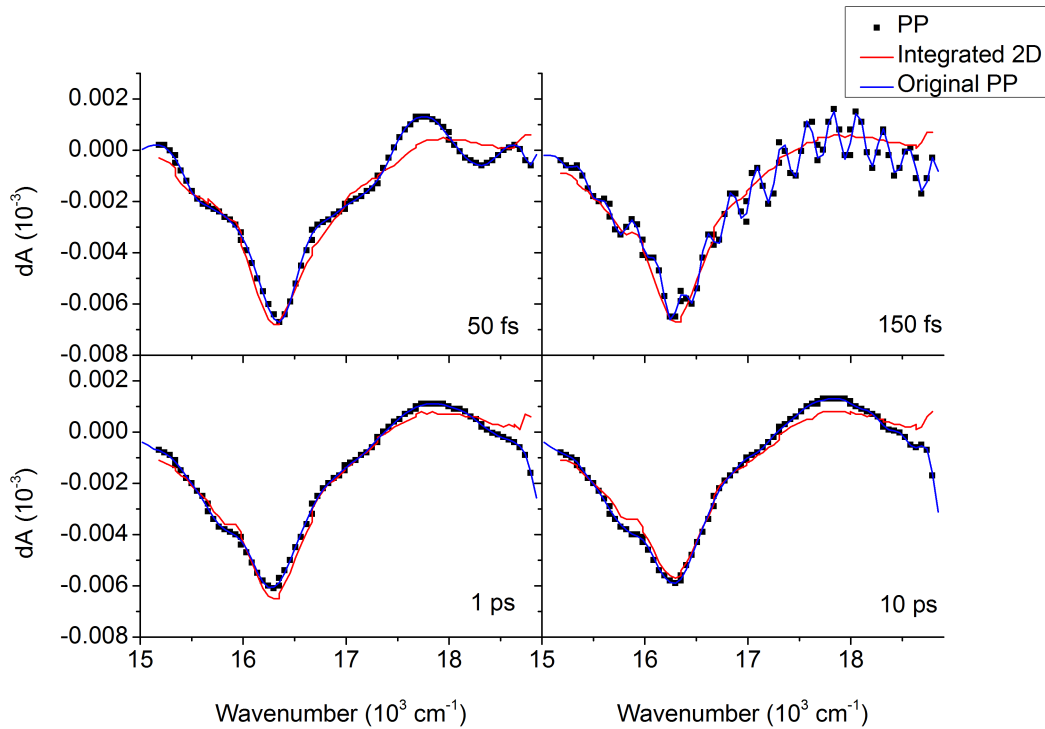
The population times were set at 5-fs intervals from 0 fs to 100 fs, then with increasing intervals according to SI-Table 1. The coherence times were scanned from -141 fs to 360 fs with 1.5-fs steps.

The data were phased by comparison to pump-probe measurements from the same setup (see SI-Figure 3). The oscillations in the pump-probe signal are caused by interference of scattered pump and probe, due to the scattering of our samples. The interference period is

SI-Table 1: Time intervals used for population times in the 2D experiments

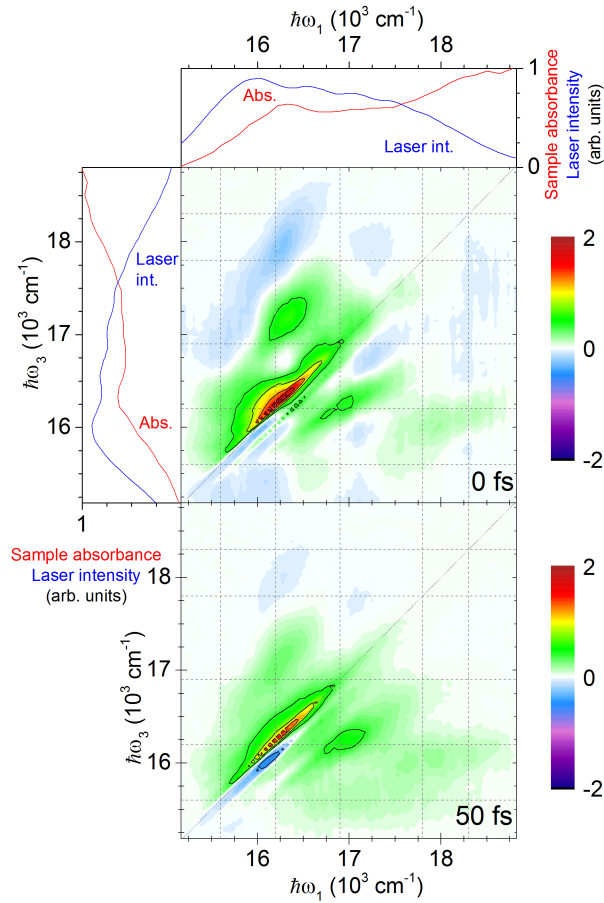
Timestep (fs)	Endpoint (fs)
5	100
10	300
40	1500
500	2000
1000	5000
5000	10000
10000	20000

getting shorter with a longer population time. Overall, it should only affect the fit to a small extent, as it is oscillating around the correct value.



SI-Figure 3: Phasing plots at selected population times.

Due to the very strong response of QDs, the nonresonant response of the glass forms only a minor contribution to the total signal, as can be seen by comparing the 0 fs and 50 fs total real spectra (SI-Figure 4; see also the 5 fs spectrum in Figure 1), unlike in many other 2DES measurements.



SI-Figure 4: Early 2D spectra (to show the small nonresonant response of the glass) with energy levels marked, laser and absorption spectra. Compare Figure 1 in the main text. Middle panel: Total real 2D spectrum of 7.1 nm CdSe QDs in methanol/ethanol glass at 77 K, at population time 0 fs. The diagonal line marks where $\hbar\omega_1 = \hbar\omega_3$; the horizontal and vertical lines mark the energy levels (see Figure 2). Bottom panel: The same, at 10 ps. Side and top panels: Sample absorbance (red line) and spectrum of the laser employed in the 2D experiment (blue line) in arbitrary units.

SI-4. Energy levels

The energy levels can be identified from the 2D spectrum or from absorption spectra, which cover a broader spectral range but have less defined peaks due to inhomogeneous broadening. At room temperature, this is combined with other sources of broadening and leads to an almost featureless spectrum. Therefore, we start by fitting the 2D data, and use the obtained state energies as a starting point in the analysis of absorption spectra. When fitting the absorption spectra, the energies of the states are kept fixed at the values of the 2D fit for the 77 K spectrum, except the two highest ones and the lowest one, which are less well defined in the 2D spectrum cut and furthermore benefit from the broader spectral range of the absorption spectra. In order to avoid the background in the absorption spectra (due to scattering and tails of high-lying unresolved bands),⁴ we subtract a linear background. At room temperature, all peaks are shifted downwards by 610 cm^{-1} compared to 77 K due to temperature dependence of the CdSe band gap.⁵ State energies are fitted globally with the temperature-dependent shift as a parameter. The obtained energies are then fed back into the 2D fit for refitting the peak widths and amplitudes, still giving a good fit and showing that the fits are consistent. A global fit of the 2D spectrum cut and the 77 K absorption spectrum was also attempted, but did not converge due to the broad, overlapping peaks in the absorption spectrum. To summarize, we can obtain a set of energy levels, which offers a consistent picture both in the 2D spectra and absorption spectra (here for both room temperature and 77 K). Apart from a low-energy weakly absorbing state, which can be assigned to the trap-related signal, all peaks are in good agreement with the energies given by Norris and Bawendi,⁴ see SI-Table 2. At 10 K, our QDs would have a first excited state energy of 2.04 eV.^{6,7}

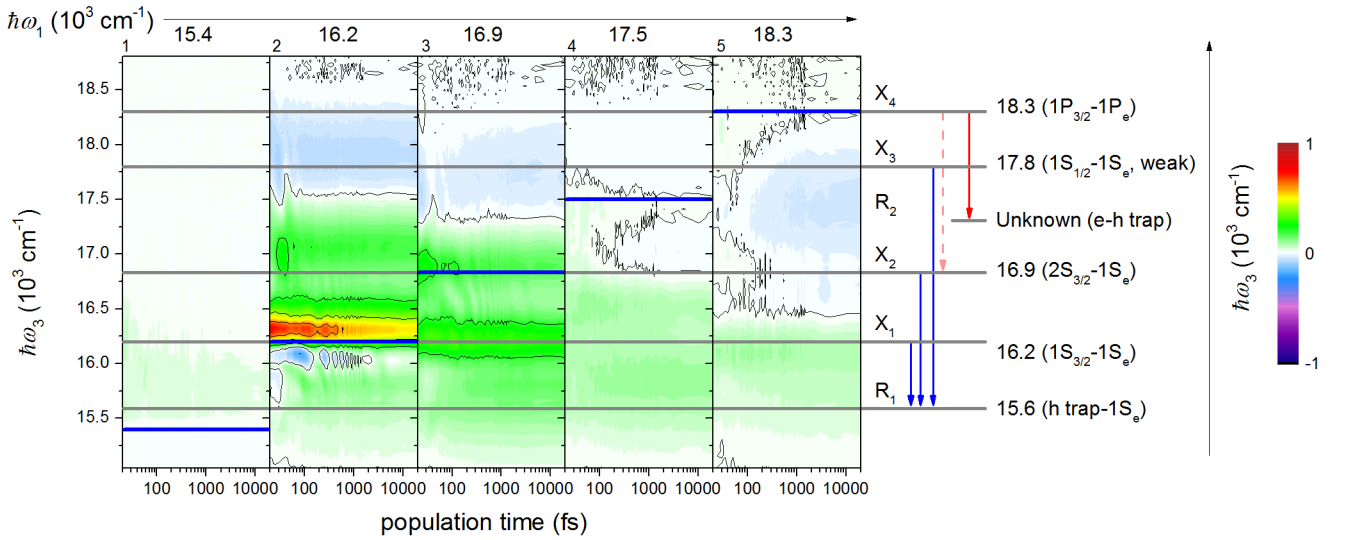
SI-5. Population dynamics

The population dynamics can be visualized in a number of different ways. In SI-Figure 5, we show how Figure 4 in the main text would look if the same normalization is used for all

SI-Table 2: Energy levels determined by us (E), their differences (ΔE) and the corresponding differences according to Norris and Bawendi (ΔE_{NB}).

E (10^3 cm^{-1})	ΔE (10^3 cm^{-1})	ΔE (eV)	ΔE_{NB} (eV)
16.2	0	0	0
16.9	0.7	0.09	0.08
17.8	1.6	0.20	0.20
18.3	2.1	0.26	0.26
19.7	3.5	0.43	0.39

slices instead of normalizing each slice to its maximum. Kinetic traces can also be obtained at single (ω_1, ω_3) points, as shown in SI-Figure 6–9.

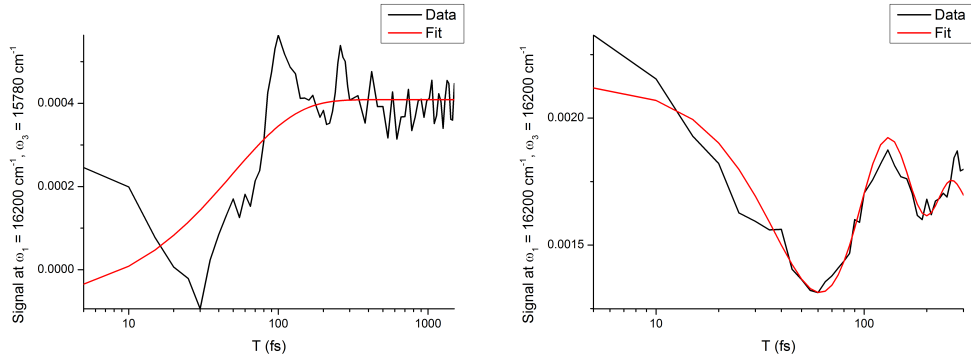


SI-Figure 5: Figure 4, using the same normalization for all panels.

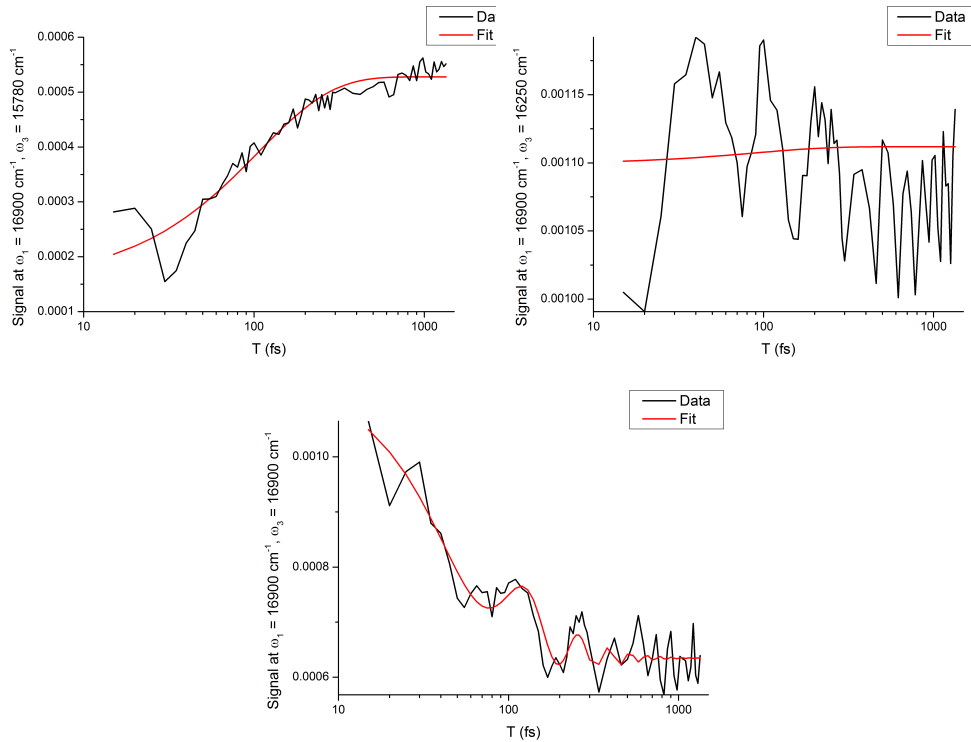
The analysis of this information leads to the decay pathways described in the main text as detailed below. Panel numbers refer to Figure 4 in the main text and SI-Figure 5.

In panel 1, we see a weak signal from the $|R_1\rangle$ state, as well as a small proportion of the signal from the $|X_1\rangle$ state due to the partial overlap of the bands. The signal from $|X_1\rangle$ shifts to $|R_1\rangle$ as the holes are trapped. $|R_1\rangle$ does not decay on this timescale.

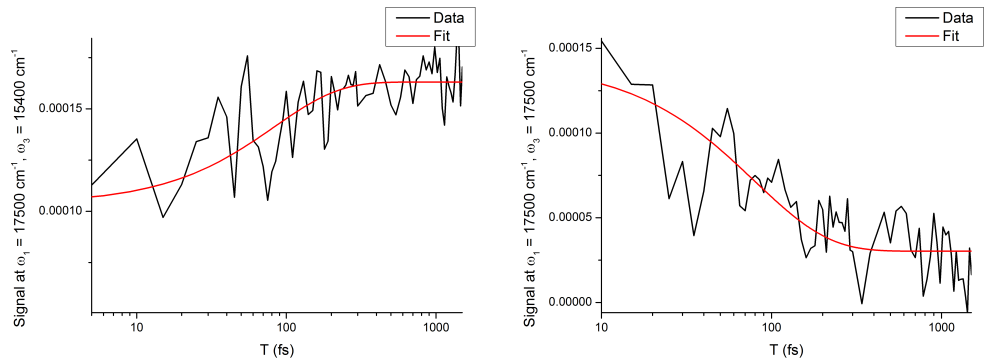
Panel 2 (dynamics after exciting $|X_1\rangle$) and panel 3 (dynamics after exciting $|X_2\rangle$) display broadly similar features. In both cases, there is a constant (on this timescale) bleach signal, caused by the presence of electrons in the $1S_e$ state, overlaid by a changing stimulated emission signal. The constant bleach signal shows that electrons remain in the $1S_e$ state



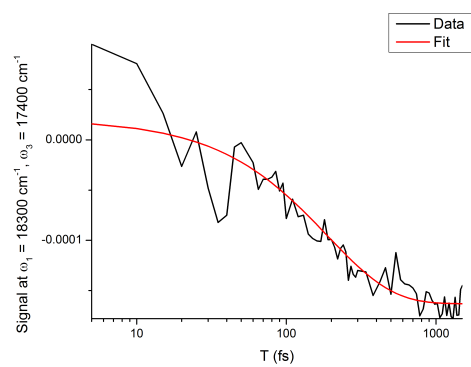
SI-Figure 6: Kinetics after exciting $|X_1\rangle$. Left: Growth of the $|R_1\rangle$ signal. Right: Decay of the diagonal peak due to equilibration between closely spaced states, phonon oscillation decay and trapping.



SI-Figure 7: Kinetics after exciting $|X_2\rangle$. Top left: Growth of the $|R_1\rangle$ signal. Top right: The signal from the $|X_1\rangle$ level is almost static, showing that holes are trapped directly from $|X_2\rangle$. Bottom: Decay of the diagonal peak.



SI-Figure 8: Kinetics after exciting $|X_3\rangle$. Left: The growth of the $|R_1\rangle$ signal. Right: Decay of the diagonal peak.



SI-Figure 9: Kinetics after exciting $|X_4\rangle$. Growth of the electron trap signal.

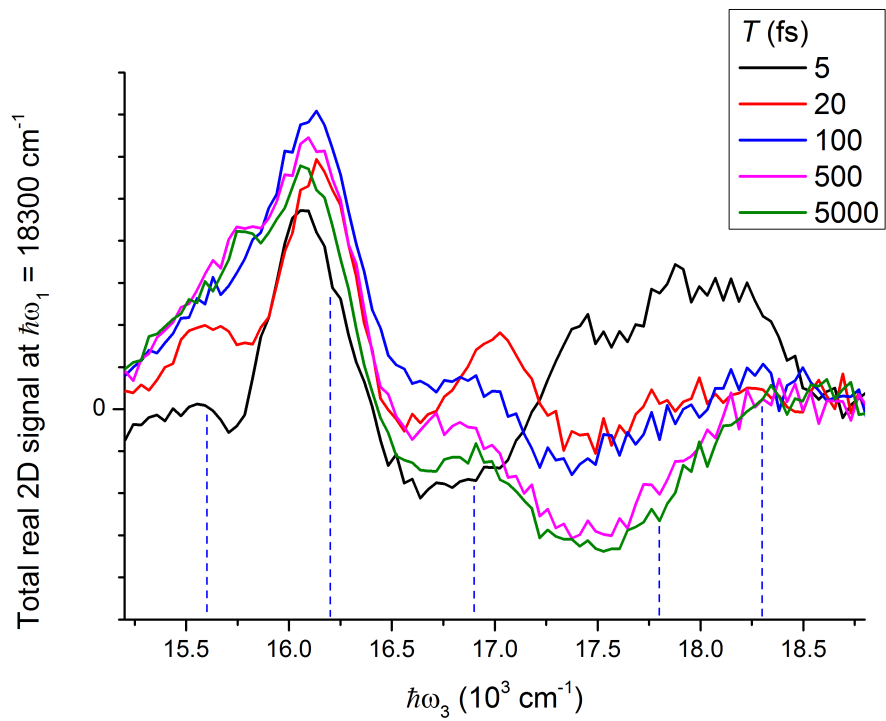
rather than being trapped, and thus that the shallow trap state is a hole trap, forming an exciton together with the $1S_e$ state.⁸ The stimulated emission signal decays from the diagonal peak ($|X_1\rangle$, right in SI-Figure 6, and $|X_2\rangle$, bottom in SI-Figure 7, respectively) and grows in at the $|R_1\rangle$ state (left in SI-Figure 6, top left in SI-Figure 7). The signal at $\hbar\omega_3 = 15600 \text{ cm}^{-1}$ in panel 2 and 3 grows in quickly (with a lifetime of $\approx 50 \text{ fs}$ for $|X_1\rangle$, slightly slower for $|X_2\rangle$, overlaid with strong oscillations due to the LO phonon modes), showing that trapping is fast.

In panel 3, the signal from the $|X_1\rangle$ level is constant (see also the top right panel of SI-Figure 7), which shows two things: firstly, that $2S_{3/2}$ holes are trapped directly without passing the $1S_{3/2}$ state, and secondly, that the share of QDs without traps is negligible. QDs without traps would cause a rise in the signal from this band due to stimulated emission. We remark that the apparent higher strength of the signal compared to panel 2 is because each panel is normalized to the maximum in the panel, and the maximum in panel 2 is higher than in panel 3 (see SI-Figure 5 for the same figure with global normalization).

In panel 4, signals are shifted to lower $\hbar\omega_3$ energies due to spectral selection of the QDs with smaller band gap to avoid overlap with the signal from the decay from $|X_4\rangle$. The pattern of decay of the diagonal peak and corresponding growth of the trap band suggests trapping directly from the $|X_3\rangle$ state as well (see SI-Figure 9). The trap band overlaps with the $|X_1\rangle$ signal. The signal at the $|X_2\rangle$ level increases faster than the decay of the diagonal peak, probably due to overlapping signal from adjoining levels.

Panel 5 is described in detail in the main text. In SI-Figure 10, we show individual spectra at $\hbar\omega_1 = 18300 \text{ cm}^{-1}$ (where relaxation from $|X_4\rangle$ dominates but $|X_3\rangle$ will also contribute) at a number of representative population times, analogous to transient absorption spectra. The diagonal peak at 5 fs has already disappeared by 20 fs, as the excited state absorption signal at 17500 cm^{-1} increases in amplitude. The growth of the excited-state absorption signal from the electron trap is shown in SI-Figure 9.

The uniform, unstructured trap band in Figure 1 does not give reason to believe that



SI-Figure 10: Spectra at a few representative population times from Panel 5 of Figure 4 and SI-Figure 5. The vertical dashed lines represent the energies of the states.

there is more than one hole trap band involved. The time constant of the hole trapping increases slightly when exciting higher states, which is consistent with a single hole trap.

References

- (1) Yu, W.; Qu, L.; Guo, W.; Peng, X. *Chem. Mater.* **2003**, *15*, 2854–2860.
- (2) Zhu, N.; Zheng, K.; Karki, K. J.; Abdellah, M.; Zhu, Q.; Carlson, S.; Haase, D.; Žídek, K.; Ulstrup, J.; Canton, S. E.; Pullerits, T.; Chi, Q. *Sci. Rep.* **2015**, *5*, 9860.
- (3) Zheng, K.; Žídek, K.; Abdellah, M.; Zhang, W.; Chábera, P.; Lemngren, N.; Yartsev, A.; Pullerits, T. *J. Phys. Chem. C* **2014**, *118*, 18462–18471.
- (4) Norris, D.; Bawendi, M. *Phys. Rev. B* **1996**, *53*, 16338–16346.
- (5) Dai, Q.; Song, Y.; Li, D.; Chen, H.; Kan, S.; Zou, B.; Wang, Y.; Deng, Y.; Hou, Y.; Yu, S.; Chen, L.; Liu, B.; Zou, G. *Chem. Phys. Lett.* **2007**, *439*, 65–68.
- (6) Varshni, Y. *Physica* **1967**, *34*, 149–154.
- (7) Joshi, A.; Narsingi, K. Y.; Manasreh, M. O.; Davis, E. A.; Weaver, B. D. *Applied Physics Letters* **2006**, *89*, 131907.
- (8) Kambhampati, P. *Chem. Phys.* **2015**, *446*, 92–107.